

A study of oxidation in thin-film uranium-niobium alloys
Logan C. Page and David D. Allred,
Department of Physics and Astronomy, Brigham Young University, Provo, UT 84602

Abstract: Uranium, a nuclear fuel material, can oxidize and degrade in reactor conditions. Previous studies have shown oxidation resistance in a uranium-niobium alloy, U-6Nb (six weight percent niobium in uranium). The nature of the oxides that form on sputtered U-6Nb thin films after long exposure to air was previously explored using neutron diffraction at Los Alamos National Laboratory. In the present work, we deposited thin films of uranium-niobium alloys for oxidation studies. We used ellipsometry to quantify the oxide growth over time as a function of niobium content. We found that the oxide thickness increases linearly with the logarithmic of time. This study also supports the hypothesis that uranium and niobium oxides form a protective passivation layer on a uranium alloy, preventing oxidation and extending the life of the fuel.

Keywords: Uranium; Niobium; Alloy; Passivation; Stainless; Oxidation; Nuclear Fuel; Uranium Oxide; Ellipsometry; Fuel Rod Degradation

1. Introduction:

Uranium is the fuel most commonly used in nuclear fission power plants around the world. However, unprotected uranium oxidizes rapidly in working ambient conditions. [1] Over time, oxidation can permeate through the entire volume of the rod. The resulting uranium oxide phases (UO_x) have an increased volume compared to pure U. This expansion can cause cracks and swelling in the volume of the fuel rod. Thus, oxidation advances corrosion. [2]

A variety of corrosion-resistant alloys, referred to as “stainless uranium”, have been found through the addition of elements such as niobium, molybdenum, and zirconium. [3] In this study, we focus on uranium-niobium (U-Nb) alloys. These alloys can be compared to stainless steel because of the passive oxide layer that forms on the surface of the alloy.

Stainless steel consists of iron (Fe) enriched with various elements, including more than 11% chromium, in a passivating oxide layer which is tens of nanometers thick, composed of chromium oxide (Cr_2O_3) on top of iron oxide. [5] The Cr_2O_3 layer retards the entry of more oxygen into the metal, thus slowing further corrosion and giving the steel its “stainless”

quality. If the oxide layer is damaged or removed, it will simply reform as the newly revealed surface oxidizes. Thus, the passivation layer is self-healing. [6]

As with stainless steel, a passive oxide layer can form on U-Nb alloys significantly slowing the oxidation process, creating a type of “stainless uranium”. To date, few studies have characterized the formation of the passivating oxide layers in U-Nb. [3,4,8,9] Analysis of the Gibbs enthalpy of oxidation in stainless steel and stainless uranium has shown that while stainless steel favors a Cr_2O_3 surface on top of iron oxide, stainless uranium instead forms UO_x on the surface, leaving an Nb-enriched area underneath to oxidize and provide a passivating barrier. [7,10]

Experimental observation of the nature of these oxides had been inconclusive, with some studies indicating an intermixed UO_2 - Nb_2O_5 oxide providing a critical Nb_2O_5 density, and others indicating chemical segregation of the UO_2 and Nb_2O_5 layers. [8,9] A recent publication by Watkins, et al. from Los Alamos National Laboratory found an interesting layer formation in U-Nb thin films via neutron reflectometry and x-ray reflectometry. They

demonstrated the long-term behavior of the passive oxide layers, finding a 31 nm thick UO_2 layer on top of a laterally undulating 5 nm Nb_2O_5 layer as shown in Fig. 1. These oxide layers created a stable equilibrium in which the underlying U-Nb alloy was not oxidized. [10]

Here, we expand upon the previous literature by investigating the formation over time of the oxide layers in a uranium-niobium alloy. After sputter-depositing a satisfactory U-Nb thin film, ellipsometry was the primary characterization tool. We intended to investigate the growth pattern of the separated oxide layers over time.

2. Methods

To observe the oxidation of the alloy over time, we deposited U-Nb thin films on silicon wafers via sputtering. Observation of new films as they aged provided data to model the alloys' oxidation over the short-term (days) and long-term (months).

Our substrates were cleaved from [100] orientation silicon test wafers coated with approximately 300 nm of chemical vapor deposition (CVD) silicon nitride on the surface. We cleaved rectangular pieces approximately 25 mm by 75 mm, to best use the space both in our sputtering chamber and our storage containers. Previous work by our group shows these wafers to have approximately 0.1 nm RMS roughness over a 1-micron-by-1-micron surface.

To prepare thin films of uranium-niobium, we used a DC-magnetron vacuum sputtering system. DC-magnetron sputtering is a physical vapor deposition (PVD) process that uses a vacuum environment to deposit thin films atom by atom. In the example shown in Fig. 2, the sputter gun is at the bottom of the vacuum chamber in “sputter up” geometry. Above the sputter gun, a substrate is placed to receive the deposited film. “Sputter up” indicates that uranium atoms are knocked out of the source at the bottom of the chamber and travel upwards towards the substrate positioned

above. The source is a thin, circular uranium plate, or target, in electrical and thermal contact with the sputter gun's high voltage cable.

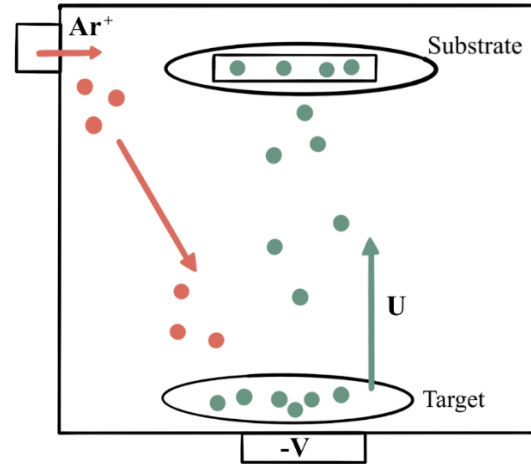


Fig. 1— Sputtering deposition process - In the sputtering deposition process, argon gas is ionized and accelerated toward the uranium target. Uranium and niobium atoms leave the target. Some land on the substrate above, forming a thin film. Figure from [12].

With the chamber in high vacuum, an inert gas like argon—called the working gas—is introduced to bring the chamber pressure to the desired level, usually about 1 mtorr. The target is biased negative DC. At sufficiently large negative voltage, the argon “breaks down” forming a plasma. In the case of magnetron sputtering, this plasma is confined near the target’s surface by strong magnets underneath the target. The plasma is slightly positive, and therefore argon atoms in the plasma are attracted to the negatively biased target. These argon atoms are accelerated towards the target by the high negative voltage between the plasma and the target to relatively high energy (about 400 eV). The energetic ions produce a cascade of collisions in the target’s surface layers. The transfer of momentum knocks some atoms out of the target, which then fly up to the substrate and accumulate a thin film.

In our vacuum sputtering system, a Meivac MAK sputter gun was at the bottom of the vacuum chamber. A 10 cm diameter depleted uranium target (material purchased from Nuclear Fuel Services, Inc) was in

electrical and thermal contact with the sputter gun. We looped niobium wires and placed them in the target's "racetrack", the most heavily eroded section, as shown in Fig. 3. Adjusting the number of wire coils allowed us to change the ratio of niobium to uranium in the deposited films. Previously we found that three loops of niobium wire produced a film of 6% weight niobium. [10] The substrate was fixed to the surface of a 4.5" platten which revolved as it rotated around the chamber in a planetary motion to promote uniform thickness over a large sample area, as is discussed in ref. [10].

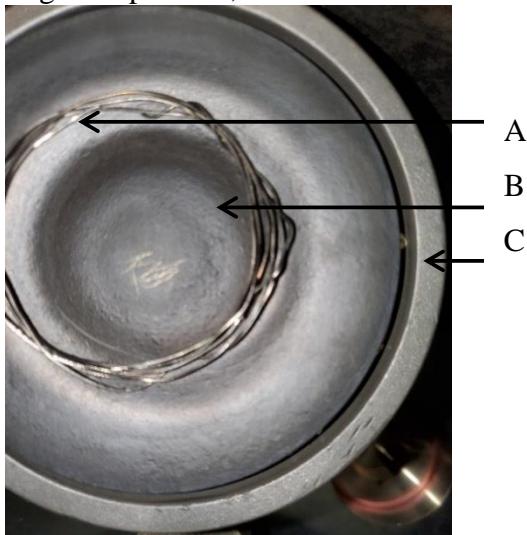


Fig. 2 – A photograph of the sputtering target and wire. A: Several loops of Niobium wire placed in the racetrack. B: Uranium target. C: Dark space shield surrounding sides of uranium target. Figure from [12].

The system's high vacuum pump was a turbomolecular pump. We evacuated our chamber until reaching high vacuum (< 0.1 mtorr) and impurities such as water vapor were pumped out of the system (as determined by a mass spectrometer). We then flowed in argon gas at a constant flow rate as controlled by a mass flow controller. With the turbopump running and argon flow, we maintained a constant pressure of about 1 mtorr as measured by a MicroPirani gauge and a 0.1 torr Baratron. We found that the plasma was stable near 1 mTorr. While the chamber was exposed to atmosphere, some oxide tended to form on the target. To avoid depositing oxidized material in

the film, we presputtered the target for several minutes to remove oxide and other impurities. During this time, the substrate was covered by rotating it inside the chamber to lie above an unused target on the opposite side of the chamber. That target was raised close to the substrate, blocking any incident sputtered particles. Once the target was cleaned of oxides, we began rotating the substrate over the target. During sputtering, the DC power supply was set to constant power. The initial power was around 450 V and 0.30 A. As time went on, the voltage decreased to about 350 V as the current increased to 0.37 A. This indicates an increase in conductance of the system over the course of sputtering, possibly due to removal of residual surface oxide. The potential and current helped identify the cleanliness of the target, as a stable current indicated a stable resistivity and a lack of oxide. With a motor controlling the rotation of the substrate, we could vary both the rotation speed and duration. Rotating the sample at $10^\circ/\text{s}$ over the plasma for nine rotations produced a film thin enough to measure with ellipsometry. Rotating for 60 rotations at the same speed produced a film so thick that deposited film began to flake off.

To characterize the samples after sputtering, we used two methods: energy dispersive X-ray analysis (EDX) and ellipsometry. EDX was primarily used to determine film composition. Ellipsometry was used to measure film thickness and index of refraction, especially as those characteristics changed over time.

EDX uses the electron beam of an electron microscope to bombard a sample's surface, stimulating x-ray emission. That is, the beam electrons collide with the sample atoms, in some cases ejecting electrons in the sample from their orbits. When an atom loses a low-energy electron, one of its high-energy electrons will transition downward to fill the hole, emitting an x ray in the process. Each element produces x rays of characteristic energies, depending on the element's electron

structure. X rays emitted from a sample are matched to characteristic x rays to determine which elements are present in what quantities. An example of these characteristic x rays is given in Fig. 4, as discussed below. Comparing the amplitude and proportion of the detected x rays allows identification and quantification of the component elements. We measured each film to determine the percentage of niobium and uranium in the film.

An EDX user is free to vary many parameters of the incident electron beam to tailor the signal to match the analytic task. An important optimization in our use of EDX was a low electron beam energy. A lower energy electron would only interact with a smaller volume near the surface. A high-energy electron penetrates more deeply into the sample, and thus interacts with both a greater depth and greater area of the sample. A high-energy electron can also excite atoms to emit higher energy x rays, allowing for a greater range of characteristic x rays to be measured. Thus, beam energy constitutes a trade-off to optimize both spatial precision and spectral range. In our measurements, we used a 5 keV electron beam for an interaction depth between 89 to 161 nm, as calculated with the Kanaya-Okayama Range Equation (Eq. 1). [11]

$$R_{KO}(nm) = \frac{27.6 A}{Z^{0.89} \rho} E_0^{1.67}$$

Eq 1 – The Kanaya-Okayama Range Equation

In this equation, A is the sample's atomic weight (g/mol), Z is its atomic number, ρ is its density, and E_0 is the electron beam energy. The constant 27.6 gives results in nanometers; 0.0276 gives microns. At 5 keV, a sample of pure uranium would have a penetration depth of 89.3 nm, and pure niobium would have a depth of 161 nm. Because our samples contain primarily uranium (>90%) and are expected to be 100 nm thick, we expected a 5 keV electron beam to interact almost exclusively with the alloy, without reaching the underlying substrate. In practice, this minimized the x ray response from the

underlying silicon nitride, although it did not entirely eliminate it.

Variable-angle spectroscopic ellipsometry (VASE) was the primary means of sample characterization. An ellipsometer measures the optical properties of a sample by measuring the change in polarization of a polarized light source after reflection at a specified angle as shown in Fig. 3. A variable-angle spectroscopic ellipsometer obtains more complete data on a sample by measuring at a series of angles over a spectrum of photon energies.

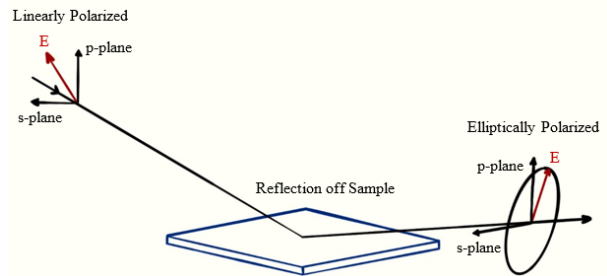


Fig 3 – Ellipsometry uses a known light source to measure the optical properties of a reflective surface.

We used a VASE ellipsometer and CompleteEASE software, both from J. A. Woollam, to measure our thin films. A key feature of the ellipsometry analysis was the interference patterns produced by the varying wavelengths of incident light at a given angle. As we produced samples, we measured them with the ellipsometer immediately after deposition. Many of the films we deposited had a metallic silver appearance implying they were too opaque to show thin-film interference from the underlying Si_3N_4 layer. A few, however, had a magenta/green color indicative of their being thin enough to permit ellipsometric use of thin film interference to precisely measure the oxidation of the alloy. [13] Our analysis focuses on one of these films.

3. Results and Discussion

Within a week of deposition (depending on electron microscope availability), we performed energy dispersive x-ray analysis on fragments of the samples (stored in atmosphere) to determine composition. EDX measurements

on the sample with 3 loops of Nb wire, taken 5 days after sputtering, revealed the composition shown in Table 1. The sample showed some evidence of carbon and oxygen, whose x-ray peaks overlap with uranium, confounding analysis. Any carbon present was most likely adventitious and/or deposited during the measurement process. Smaller amounts of nitrogen and silicon were also observed, indicating that the interaction volume of the microscope's electron beam exceeded the thickness of the film and passed through to the underlying Si_3N_4 layer. Since our aim is to determine the ratio of niobium to uranium in the film, we renormalized the measurements including only the niobium and uranium components.

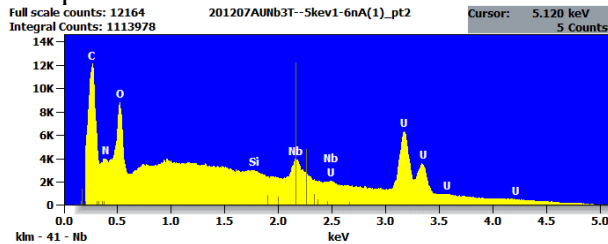


Fig. 4 – EDX spectrum of the 3-loop UNb film, with a nominal ellipsometric thickness of 150 nm. Figure from [12].

Table 1 – EDX measurements 5 days after sputtering show the sample produced from 3 loops of Nb wire to contain 3.92% weight Nb after renormalization. Table from [12].

	N	O	Si	Nb	U
Weight %	0.74	1.30	0.23	3.80	93.10
Atomic %	8.26	12.64	1.30	6.37	60.88
Renormalized Weight %				3.92	96.08
Renormalized Atomic %				9.47	93.89

This same “3-loop” sample was purple in appearance and showed measurable interference fringes through measurement. This means the film was quite transparent so that its color was determined by the interference of the underlying Si_3N_4 film with the Si substrate. The film also had a similar composition to the

sample used by Watkins et al. We therefore focused our ellipsometric thickness measurements on this film.

We measured the film repeatedly at increasing intervals over the course of months. We then fit the data to an optical model representing different layers in the film. The model that best fit the data included a series of three distinct layers. Namely, uranium oxide, niobium oxide, and uranium-niobium alloy. This is shown in Table 2 and Fig. 5. See also fig. 4 of ref. 10. Not shown is the 300 nm layer of silicon nitride below. According to this model, the thickness of the niobium oxide and uranium oxide layers increased logarithmically with time. The thicknesses estimated by this model seem too large. Other films we produced that were too opaque were also in the 100 nm thickness range, so we believe this sample to be thinner than it appears. We suspect inaccuracies in the optical constants of our model. However, these have not been sufficiently investigated. Therefore, we are use 150 nm as the nominal thicknesses. The figure shows a logarithmic oxide growth, which agrees with the work of Watkins et al. in determining a long-term oxide state for similar films. A more extensive discussion of this can be found in reference 12.

In this model, the uranium moved outward as it oxidized. The niobium oxide grew under the uranium oxide, directly on top of the original uranium-niobium alloy. As seen in Fig. 7, the uranium oxide was much thicker than the niobium oxide; this is likely the result of the

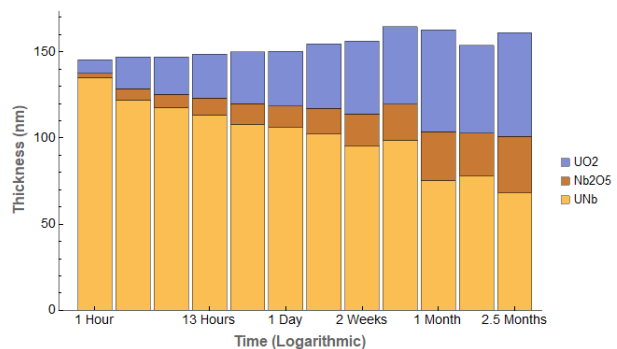


Fig. 5 – The oxide layers’ thickness over time. UO_2 migrated to the outside; Nb_2O_5 underneath, on top of the UNb alloy.

Table 2 - Thickness of thin-film layers over time, as measured with ellipsometry. Data drawn from reference 12.

Oxide Layer Thickness Over Time												
Time (mins)	80	285	500	780	1600	2160	6500	19000	38000	56000	65000	110000
UO ₂ Thickness (nm)	7.97	18.49	21.75	25.61	30.09	31.65	37.64	42.48	44.97	59.13	50.86	60.06
Nb ₂ O ₅ Thickness (nm)	2.44	6.66	7.53	9.64	11.8	12.5	14.81	18.53	20.94	28.03	24.98	32.83
UNb Thickness (nm)	135.13	122	117.74	113.39	108.02	106.08	102.32	95.36	98.64	75.59	77.96	68.11

original ratio of uranium to niobium in the alloy. The logarithmic slowing of the oxidation left the internal uranium-niobium alloy unoxidized only tens of nanometers under the surface. This follows the expected behavior of the passivation layer, retarding the oxidation of the alloy.

3. Summary and Conclusions

The observed uranium and niobium oxide layers that formed retarded the long-term oxidation of the alloy. They followed the logarithmic law as shown in ref 12. This slowing provides evidence that the films act as a passivation layer on “stainless uranium”. A notable difference from stainless steel was observed, however. As explained previously, stainless steel passivates as chromium oxide forms on the outer surface. In our alloy, the passivation layer of niobium oxide formed *underneath* the uranium oxide rather than on top. This indicates that the oxidation layers in the uranium-niobium alloy may differ from those that form on stainless steel. This includes quite different Gibbs energy, as was noted. The key result, however, is clear: since the alloy shows a slowing rate of oxidation with time, the uranium/niobium oxides create an oxidation-resistant passivation layer.

Further work is justified to investigate the nature of oxide formation on alloys with various other proportions of niobium in uranium.

4. Acknowledgments

This publication is largely based on Logan C. Page’s senior thesis.[12] Research was partially supported by the College of Physical and Mathematical Sciences and Department of Physics and Astronomy at Brigham Young

University. Mr. Page also acknowledge scholarship support from the Utah NASA Space Grant Consortium. We grateful to Erik Watkins and Jaroslaw Majewski at Los Alamos National Laboratory for helpful conversations. BYU students Josh Vawdrey and Kenan Fronk also contributed to this project.

References:

1. Idriss, H., *Surface reactions of uranium oxide powder, thin films and single crystals*. Surface Science Reports, 2010. **65**(3): p. 67-109.
2. McEachern, R.J. and P. Taylor, *A review of the oxidation of uranium dioxide at temperatures below 400 degrees C*. Journal of Nuclear Materials, 1998. **254**(2-3): p. 87-121.
3. Manner, W.L., et al., *An examination of the initial oxidation of a uranium-base alloy (U-14.1 at.% Nb) by O-2 and D2O using surface-sensitive techniques*. Applied Surface Science, 1999. 150(1-4): p. 73-88.
4. Fu, X.G., et al., *X-ray photoelectron spectroscopic study of the surface reaction of uranium-niobium alloy with O-2*. Surface Review and Letters, 2003. 10(2-3): p. 381-386.
5. Olsson, C.O.A. and D. Landolt, *Passive films on stainless steels - chemistry, structure and growth*. Electrochimica Acta, 2003. 48(9): p. 1093-1104.
6. Maurice, V. and P. Marcus, *Progress in corrosion science at atomic and nanometric scales*. Progress in Materials Science, 2018. 95: p. 132-171.
7. Knacke, O., O. Kubaschewski, and K. Hesselmann, *Thermochemical properties of inorganic substances*. 1991, Berlin; New York; Düsseldorf: Springer-Verlag ; Verlag Stahleisen.
8. Kelly, D., et al., *Surface characterization of oxidative corrosion of U-Nb alloys*. Journal of Vacuum Science & Technology a-Vacuum Surfaces and Films, 2001. 19(4): p. 1959-1964.

9. Embong, Z., et al., *In situ study of the initial stages of oxidation of alloy U-6wt.% Nb with angle resolved x-ray photoelectron spectroscopy (ARXPS)*. Journal of Science and Technology, 2009. 1(1): p. 43-55.
10. Watkins, Erik B. et al., *Oxide structure of air-passivated U-6Nb alloy thin films*, Journal of Nuclear Materials, 2020, **539**, 152356.
11. Goldstein, Joseph, et al., *Scanning electron microscopy and x-ray microanalysis*. 2003, New York.
12. Page, Logan Coleman. “*Stainless Uranium*” - *Oxidation Prevention in Uranium-Niobium Alloys*, Senior thesis, 2021. <https://physics.byu.edu/docs/thesis/1486>
13. Johnson, Brian I., Avval, Tahereh G., Turley, R. Steven, Linford, M. R., Allred, D. D., *Oxidation of aluminum thin films protected by ultrathin MgF2 layers measured using spectroscopic ellipsometry and x-ray photoelectron spectroscopy*,” OSA Continuum 4(3), 879-895 (2021). <https://doi.org/10.1364/OSAC.417302>

Appendix A

A.1 Stepper Motor Controller Design with Phidget®

The following is a Python program we wrote to operate the Phidget Stepper Motor Controller Model 1063_1 which rotated our substrate during sputtering. In writing, we drew from several sources including Phidget documentation, Tkinter documentation, and StackOverflow.com. The program produces a windowed Graphical User Interface (GUI) that accepts inputs for rotation speed, number of rotations, and rotation direction, and outputs the motor’s actions in a text box.

```
# -*- coding: utf-8 -*-
"""
Created on Fri Sep 4 19:08:09 2020
GUI that can control the Phidget Stepper Motor
@author: Logan Page
"""
import tkinter as tk
import sys
from Phidget22.Phidget import *
from Phidget22.Devices.Stepper import *
from Phidget22.Devices.DigitalInput import *
from Phidget22.Devices.CurrentInput import *
import threading

#Print window definition
class PrintLogger(): # create file like object
    def __init__(self, textbox): # pass reference to text widget
        self.textbox = textbox # keep ref

    def write(self, text):
        self.textbox.insert(tk.END, text) # write text to textbox
        self.textbox.see(tk.END) # scroll to end of textbox to
        make new lines always visible

    def flush(self): # needed for file like object
        pass

def rotate():
    if stepper0.getIsMoving()==True:
        stepper0.setVelocityLimit(0)

vel=ent_runspeed.get()
rots=ent_rotations.get()
direction = var_direction.get()

#check valid input
if len(vel)==0:
    print('Input desired velocity.')
    return
if len(rots)==0:
    print('Input desired rotations.')
    return

vel=int(vel)
rots=int(rots)

if direction==True:
    direct = "backward";
    int_direct=-1;
else:
    direct="forward";
    int_direct=1;

#Seconds per rotation
global rotlength
rotlength = 360/vel

#Timer for full run
global timer
timer = threading.Timer(360*rots/vel, stopRotation)

#Timer to count individual rotations
global countrotationtimer
countrotationtimer = threading.Timer(rotlength,
countRotation)
```

```

global counter
counter = 0

print("Turning ' + str(direct) + ' at ' + str(vel) + '°/s for ' +
str(rots) + ' turns.')
stepper0.setVelocityLimit(int_direct*vel)
stepper0.setEngaged(True)
timer.start()
countrotationtimer.start()

def stopRotation():
    print('Stopping')
    stepper0.setVelocityLimit(0)
    stepper0.setEngaged(False)
    global timer
    if(timer is not None):
        timer.cancel()
    global countrotationtimer
    if(countrotationtimer is not None):
        countrotationtimer.cancel()
    global counter
    counter = 0

def onAttach(self):
    print("Attached!")

def onDetach(self):
    print("Detached!")

def countRotation():
    global counter
    global countrotationtimer
    global rotlength
    counter += 1;
    print(str(counter))
    countrotationtimer.cancel()
    countrotationtimer = threading.Timer(rotlength,
countRotation)
    countrotationtimer.start()

#Timer for setting rotation count
global timer
timer = None
global countrotationtimer
countrotationtimer = None
#Create a new stepper controller channel
stepper0 = Stepper()

#General Window/Frame Setup
window=tk.Tk()
window.title("Phidget Stepper Control")
window.geometry("425x400")

frm_buttons = tk.Frame(master=window)
frm_buttons.grid(row=1,column=0,sticky="nesw",padx=10,pad
y=10)
frm_buttons.grid_columnconfigure((0,1,2,3),weight=1)
#needed for centering

frm_info = tk.Frame(master=window)
frm_info.grid(row=0,column=0,sticky="nesw",
padx=10,pady=10)
frm_info.grid_columnconfigure((0,1,2,3),weight=1)#needed
for centering

#Establish input options
lbl_runspeed = tk.Label(master=frm_info, text = "Degrees/sec:
")
ent_runspeed = tk.Entry(master=frm_info, width=10)
lbl_runspeed.grid(row=0, column=1,pady=10)
ent_runspeed.grid(row=0, column=2,pady=10)

lbl_rotations = tk.Label(master=frm_info, text = "# Rotations:
")
ent_rotations = tk.Entry(master=frm_info, width=10)
lbl_rotations.grid(row=1, column=1,pady=10)
ent_rotations.grid(row=1, column=2,pady=10)

var_direction = tk.IntVar()
check_direction = tk.Checkbutton(master=frm_info,
text="Reverse", variable=var_direction)
check_direction.grid(row=3, column=2,padx=10,pady=10)

#Establish buttons
btn_go = tk.Button(master=frm_buttons, text = "GO", width =
10, height = 3, bg="green", command = rotate)
btn_stop = tk.Button(master=frm_buttons, text = "STOP",
width = 10, height = 3, bg='red', command = stopRotation)

btn_go.grid(row = 0, column = 1)
btn_stop.grid(row = 0, column = 2)

#Establish Output window
frm_output = tk.Frame(master = window)
frm_output.grid(row = 2, column = 0, sticky = "nesw", padx =
10, pady = 10)
outputwindow = tk.Text(master = frm_output, width = 50,
height = 9)
outputwindow.pack()

# create instance of file like object
pl = PrintLogger(outputwindow)

#address digital channels
stepper0.setDeviceSerialNumber(130307)

#Assign event handlers
stepper0.setOnAttachHandler(onAttach)
stepper0.setOnDetachHandler(onDetach)

#Open and wait for attachment
if(stepper0.getAttached()):
    stepper0.close()
stepper0.openWaitForAttachment(3000)

#For degrees, = 360/(CPR*encoder res*gear ratio). we couldn't
find the motor specs so we guessed. It's wrong by a little.
stepper0.setRescaleFactor(360/(6475))
stepper0.setControlMode(StepperControlMode.CONTROL_M
ODE_RUN)

# replace sys.stdout with our object

```



```
default_stdout = sys.stdout
sys.stdout = pl

window.mainloop()
```

```
sys.stdout = default_stdout
#close channel
stopRotation()
stepper0.close()
```

A.2 PyInstaller Setup File

The following is a Python program we wrote to convert the GUI Python code into an executable file using PyInstaller. In writing we edited an example from the PyInstaller documentation. The Python code file's location is input, as well as options to make it a single file which opens a windowed program. Running the file produces an EXE file, as well as a "build" folder which can be deleted.

```
# -*- coding: utf-8 -*-
"""
```

```
Created on Tue Mar 23 13:08:28 2021
```

```
Short code to create EXE from python code, copied from PyInstaller documentation.
```

```
@author: Logan Page
```

```
"""
```

```
import PyInstaller.__main__
```

```
PyInstaller.__main__.run([
    'C:\\Users\\DrAllredLab\\PhidgetGUI-Working.py',
    '--onefile',
    '--windowed'
])
```